P5.1 VARIATIONAL ASSIMILATION OF SSM/I OBSERVATIONS IN CLEAR SKIES AT THE METEOROLOGICAL SERVICE OF CANADA

David Anselmo* and Godelieve Deblonde
Meteorological Service of Canada

1 INTRODUCTION

At the Canadian Meteorological Centre (CMC), improvements in the global analyses and forecasts in recent years have largely been realized as a result of an increased assimilation of satellite data. Since March of 2005, the CMC global analyses are generated using a 4D-Var assimilation scheme which assimilates conventional data (e.g. radiosonde, aircraft, wind profilers), satellite derived automated motion vectors, and satellite radiances (GOES-W, GOES-E, AMSU-A aboard NOAA-15, -16, and AQUA, and AMSU-B aboard NOAA-15, -16, and -17).

One of the anticipated changes to the operational analysis system over the coming year is the addition of Special Sensor Microwave Imager (SSM/I) data. In preparation for this, experiments are conducted to satisfy two primary objectives. The first is to determine the impact of the assimilation of SSM/I brightness temperatures in clear-skies and over open oceans. The second is to test a stricter filtering regime for the AMSU data currently assimilated. The motivation for the latter modification will be discussed in the subsequent section. This will be followed by a description of the experiment setup, the results of the experiments, and the conclusions.

2 MODIFICATIONS TO THE SELECTION PROCESS FOR AMSU DATA

Currently, the CMC assimilates from the AMSU-A instrument channels 3 through 10 over oceans and channels 6 through 10 over land (see Table 1). Observations in precipitating and cloudy regions are filtered using algorithms (Grody et al. 2001) which compute the scattering index and cloud liquid water (CLW) amount, respectively. The CMC's variational analysis system is not capable of assimilating cloudy observations since CLW is not an analysed variable and, moreover, the radiative transfer model assumes that CLW is zero. The cloud filter employed removes pixels with a CLW value greater than 0.3 mm. However, AMSU-A channel 3 exhibits a moderate sensitivity to clouds (Fig. 1), which strongly suggests that the 0.3 mm threshold is not sufficiently low to properly remove observations affected by moisture. The danger is that a bias in the water vapour field might be introduced where observations in cloudy, non-precipitating regions are assimilated since a higher brightness temperature would induce a larger humidity value in the analysis. For this reason, in the second experiment all observations from AMSU-A channel 3 are eliminated from the assimilation process.

Channel No.	Frequency (GHz) / Polariz. at Nadir	Resolution (km)	Assimilation
AMSU-A			
1	23.8 V	48	No
2	31.4 V	48	No
3	50.3 V	48	Ocean
4	52.8 V	48	Ocean
5	53.596 H	48	Ocean
6	54.4 H	48	Ocean/Land
7	54.94 V	48	Ocean/Land
8	55.5 H	48	Ocean/Land
9	57.29 H	48	Ocean/Land
10	57.29 H	48	Ocean/Land
11	57.29 H	48	No
12	57.29 H	48	No
13	57.29 H	48	No
14	57.29 H	48	No
15	89.0 V	48	No
AMSU-B			
1	89.0 H	16	No
2	150.0 H	16	Ocean
3	183.31 H	16	Ocean/Land
4	183.31 H	16	Ocean/Land
5	183.31 H	16	Ocean

Table 1. AMSU channel properties and their operational assimilation at MSC.

From the AMSU-B instrument, channels 2 through 5 are assimilated over oceans and channels 3 and 4 over land (Table 1). A precipitation screen based on the scattering index algorithm developed by

* *Corresponding author address:* David Anselmo, Meteorological Service of Canada, 2121 Trans-Canada Highway, Dorval, Québec, Canada H9P 1J3; e-mail: David.Anselmo@ec.gc.ca

Bennartz et al. (2002) removes rainy observations. However, there is no cloud filter present. Due to the moderate sensitivity of AMSU-B channel 2 to clouds (Fig. 2), this channel is subjected to additional filtering in the second of our experiments. This enhanced filtering is also applied to AMSU-B channels 3 through 5, in response to their small sensitivity to clouds at mid-levels (Fig 2.). This filter is essentially a pseudo cloud filter, and it is the same as that applied at Meteo-France and the European Centre for Medium-Range Weather Forecasts (ECMWF). It removes AMSU-B observations over oceans where the absolute difference between the observed and background brightness temperatures for AMSU-B channel 2 exceeds 5 K.

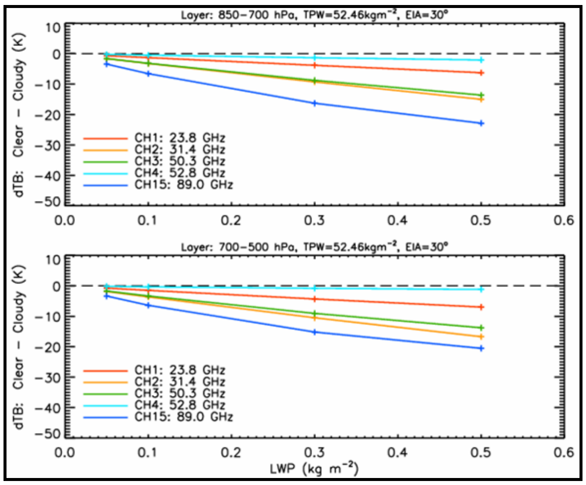

Figure 1. Sensitivity of AMSU-A channels to clouds (LWP = Liquid Water Path in kg m^{-2}).

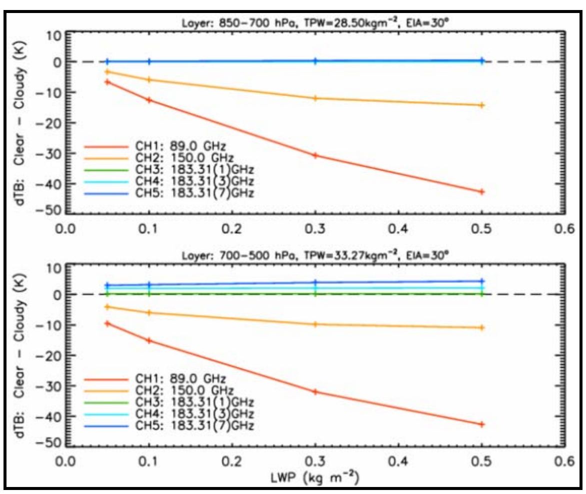

Figure 2. Sensitivity of AMSU-B channels to clouds (LWP = Liquid Water Path in kg m^{-2}).

3 EXPERIMENT SETUP

The experiments are executed over two five week periods during the northern hemisphere (NH) summer of 2003 (June 24th to July 31st) and winter of 2004 (December 25th to January 31st) To avoid any spurious effects that can occur when changes are made to the assimilation system, the first week of analyses are discarded in both cases. Control simulations (CNT1) are produced using the same configurations that were employed operationally during July 2003 and January 2004. Over these periods the 3D-Var assimilation scheme was active and the trial fields were produced using the CMC's 0.9^{o} resolution global model with 28 terrain-following vertical levels (Côté et al. 1997). The conventional observations included in CNT1 are from surface, radiosonde, dropsonde, and aircraft sources. Input data also consists of the direct assimilation of radiances from the GOES-W geostationary satellite and brightness temperatures from the AMSU-A and AMSU-B instruments aboard the NOAA-15, -16, and -17 polar orbiters. For January 2004, data was no longer available from the NOAA-17 AMSU-A after the instrument suffered catastrophic failure in October 2003.

Channel No.	Frequency (GHz)	Resolution (km)	Assimilation
1	19.35 V	25	Ocean
2	19.35 H	25	Ocean
3	22.235 V	25	Ocean
4	37.0 V	25	Ocean
5	37.0 H	25	Ocean
6	85.5 V	12.5	Ocean
7	85.5 H	12.5	Ocean

Table 2. SSM/I channel properties and their experimental assimilation at MSC.

The first experiment, EXP1, is produced by adding clear-sky, open-ocean observations from the SSM/I instruments aboard the Defense Meteorological Satellite Program (DMSP) satellites (DMSP-13, DMSP-14, DMSP-15) to the CNT1 setup. All seven channels of SSM/I, whose frequencies and polarizations are defined in Table 2, are assimilated. Observations in cloudy and precipitating regions are removed using algorithms following Alishouse et al. (1990), Petty (1990), and Weng and Grody (1994). The SSM/I is an imager, and therefore, provides indirect information on vertically integrated quantities such as IWV and CLW. The horizontally polarized channels also show a moderate sensitivity to SWS. It is not characterized by a strong sensitivity to air temperature. In the second experiment, henceforth labeled EXP8, the SSM/I data is added while select AMSU data is removed. This refers to the complete rejection of AMSU-A channel 3, as well as the application of the pseudo cloud filter to AMSU-B channels 2, 3, 4, and 5, as described in the previous section. Both AMSU and SSM/I brightness temperatures are bias corrected using an algorithm based on that developed by Harris and Kelly (2001).

The analyses generated from each of the cycles are studied using monthly averaged fields of integrated water vapour (IWV), derived from the Advanced Microwave Scanning Radiometer (AMSR-E) aboard the AQUA spacecraft, and surface wind speed (SWS) from QuikScat. These independent data sets are made available by Remote Sensing Systems (http://www.remss.com). Daily precipitation rates (DPR), computed by accumulating the 6-hr forecast amounts extracted from the trial fields, are evaluated using observed values from the Global Precipitation Climatology Project (GPCP). GPCP data is available from the National Climatic Data Center via the internet. Ten-day forecasts for each of the cycles are validated using both radiosonde observations (RAOBS) and analyses from the same experiment. As part of the validation, standard deviation (SD), root mean square (RMS) error, bias, and anomaly correlation (AC) statistics are generated. Finally, quantitative precipitation forecasts (QPFs) over North America are verified using 2 categorical measures – bias and equitable treat score.

4 EXPERIMENT RESULTS

4.1 Comparing analyses against independent observations

4.1.1 AMSR-E IWV

For the July experiments, a comparison of the zonally averaged analyses of IWV for the month of July against that observed by the AMSR-E reveals strong improvements in the SD, correlation (CORR), and bias, particularly in the NH (Fig. 3). Most of the improvement is due to the addition of SSM/I data, however, further gains are made in all the statistics as a result of the changes made to the AMSU data assimilated. With respect to the bias, in both experiments there is an addition of moisture in the NH and a reduction in the southern hemisphere (SH), both of which reduce the bias.

For the January experiments, the same comparison shows improvements in the SD and CORR for both EXP1 and EXP8 over CNT1, mainly in the tropics and SH (Fig. 4). A positive bias in tropical regions has increased as a result of a reduction in moisture in both cases. Since the curves for EXP1 and EXP8 are very close, it is concluded that almost all the impact is attributed to the addition of SSM/I data alone.

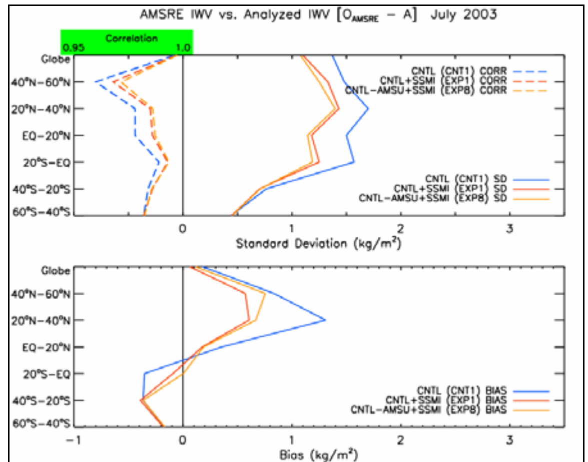

Figure 3. Monthly mean IWV (kg m^{-2}) from the analyses compared against that observed by AMSR-E for July 2003. The top diagram shows correlation in dashed lines on the left and standard deviation in solid lines on the right. The bottom diagram shows bias. AMSR-E data is provided by Remote Sensing Systems (src: www.remss.com).

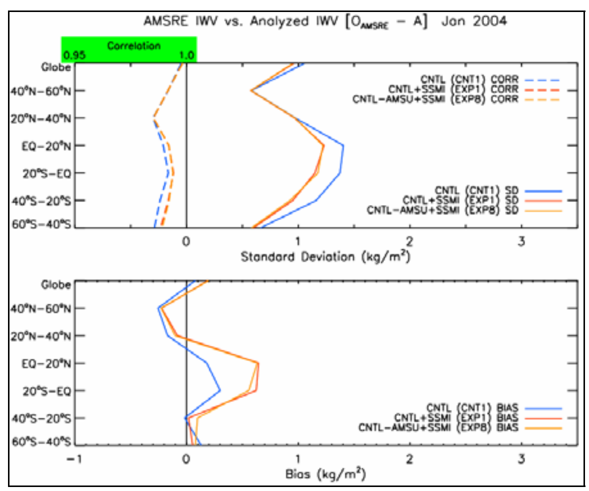

Figure 4. Same as in Figure 3, except for January 2004.

4.1.2 QuikScat SWS

In July and January the effect of both experiments on SD and CORR is small and positive, again with almost all of the impact attributed to the addition of SSM/I data (Fig. 5 and 6). With regards to bias, in the NH a deterioration is observed in July and an improvement in January. In the SH for July, removing select AMSU data has offset some of the gains made by the addition of SSM/I data which had increased surface wind speed to more closely match that observed by QuikScat. Over the SH circumpolar ocean, the operational analysed winds are generally underestimated.

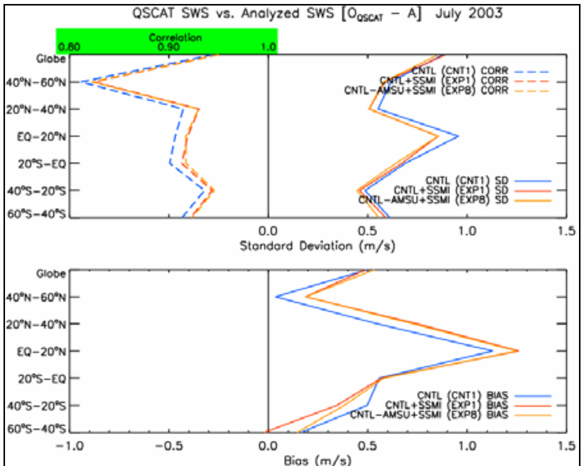

Figure 5. Monthly mean SWS (m s^{-1}) from the analyses compared against that observed by QuikScat for July 2003. The top diagram shows correlation in dashed lines on the left and standard deviation in solid lines on the right. The bottom diagram shows bias. QuikScat data is provided by Remote Sensing Systems (src: www.remss.com).

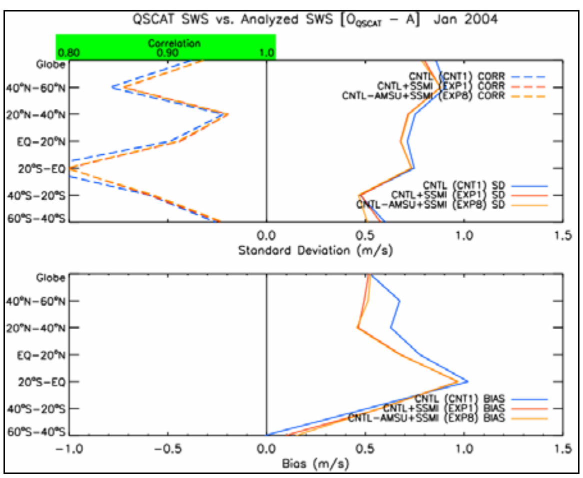

Figure 6. Same as in Figure 5, except for January 2004.

4.1.3 GPCP DPR

In July, improvements in all statistical categories are evident in the tropics for EXP1 (Fig. 7). The impact is even more positive for EXP8, demonstrating an advantage to the enhanced filtering of AMSU data.

In January, there is essentially no change to the curves (Fig. 8).

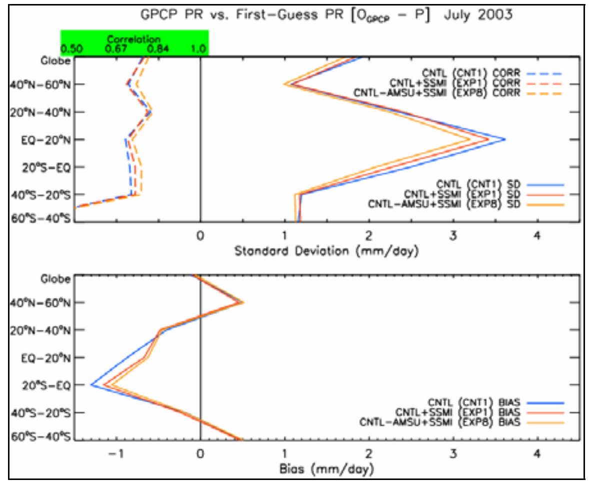

Figure 7. Comparison of monthly mean DPR (mm day^{-1}) computed from 6h forecasts compared against GPCP values for July 2003. The top diagram shows correlation in dashed lines on the left and standard deviation in solid lines on the right. The bottom diagram shows bias. GPCP data is provided by the National Climatic Data Center (src: http://lwf.ncdc.noaa.gov/oa/wmo/wdcamet-ncdc.html).

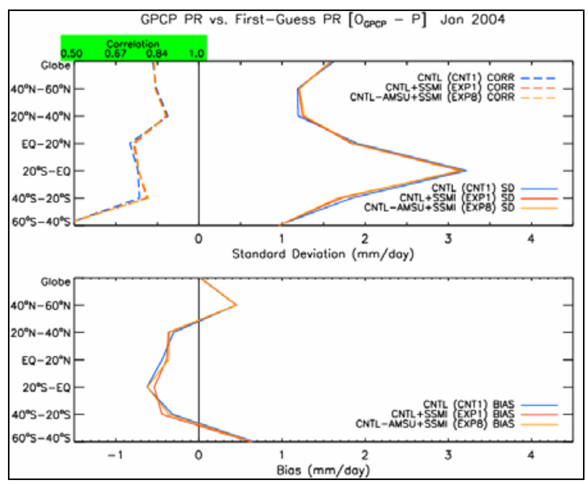

Figure 8. Same is in Figure 7, except for January 2004.

4.2 Verification of forecasts against RAOBS

To gauge the effects of the new configurations on the forecasts, comparisons of the predicted meteorological fields of geopotential (GZ), temperature (TT), total wind (UV), zonal wind (UU), and dewpoint depression (ES) are made against RAOBS. Vertical profiles of the bias and SD are studied for the forecast ranges from T+0h to T+240h in 24h increments.

In the validation of the forecasts of EXP1 it is found that the effect is essentially neutral for both seasons. This is somewhat surprising considering the improvements in the analysed fields that were discussed in the previous sub-section. However, since SSM/I data is assimilated only over oceans and the majority of RAOBS are land-based, the impact would be expected to be muted to a large degree. This issue is discussed further in subsequent sections.

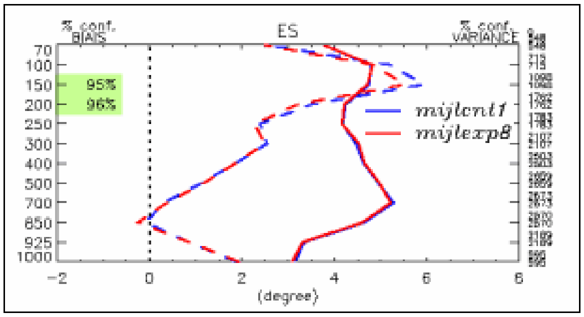

Figure 9. The 6h forecasts of dewpoint depression (ES) from CNT1 (blue) and EXP8 (red) validated against RAOBS in the SH for July 2003. Variance is plotted in solid lines and bias in dashed lines. The percentages in green boxes indicate statistical confidence.

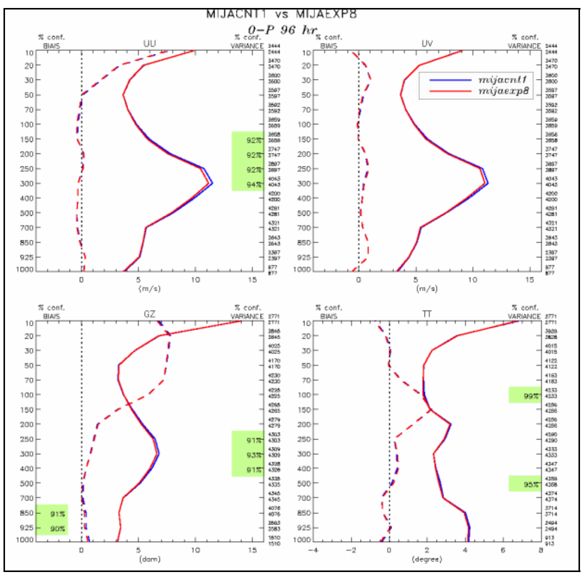

Figure 10. Same as in Figure9, except for the 96h forecasts of zonal wind (UU), total wind (UV), geopotential (GZ), and temperature (TT) validated against RAOBS in NA for January 2004.

For EXP8, the overall impact is small, but almost entirely positive for both July and January. Perhaps the most notable improvement is a reduction in bias for atmospheric humidity in the layer between 100 and 200 hPa over the SH for the month of July (Fig. 9). The effect appears in the comparison of the 6h forecast to RAOBS and persists to 144h of integration. This gain may be attributed to the improved quality control applied to AMSU-B CH3, which shows maximum sensitivity to moisture near the tropopause.

Beyond the 120h forecasts, the July results are generally neutral, however, for some fields the impact alternates between weak positive and weak negative. In January, several improvements in GZ and UV are evident in the NH and in NA from T+96h to T+240h (e.g. Fig 10).

4.3 Verification of forecasts against RAOBS time series

In the previous section, mean statistics computed over a one month period were studied. To better evaluate the performance of the forecasts on a day-to-day basis, time series of the bias and SD of forecast values of GZ, UV, TT, and ES versus RAOBS are plotted at several vertical levels for the months of July and January. These charts indicate whether important forecast busts are avoided or added by the new setup of an experiment.

Generally, for both experiments and for both seasons, the RAOBS time series plots do not indicate notable positive or negative effects as a result of the changes made to the assimilation system. This is true for all meteorological fields and for all the vertical levels over several sub-regions of the globe.

4.4 Verification of forecasts against analyses

The impact on the forecasts may also be assessed by verifying them against their corresponding analyses. This is done using RMS error and AC statistics. Overall, in both seasons the impact of EXP1 is neutral while that of EXP8 is somewhat positive.

For July 2003, improvements associated with EXP8 are observed in GZ and TT AC in the lower troposphere of the tropics (e.g. Fig. 11). This is true as well for the RMS error of near-surface moisture in the NH (Fig. 12). A reduction of RMS error in ES at 100 hPa in the SH (Fig. 13) agrees well with the positive impact previously illustrated in the bias statistics of the RAOBS charts. Improvements are also observed in the near-surface tropical winds for both experiments (Fig. 14). In terms of negative impact, degradation in the moisture field is found in the SH 850 hPa RMS error (Fig. 15), in the 700 hPa RMS error over North America (NA) (Fig. 16), and in the 100 hPa RMS error in the tropics (Fig. 17). In the

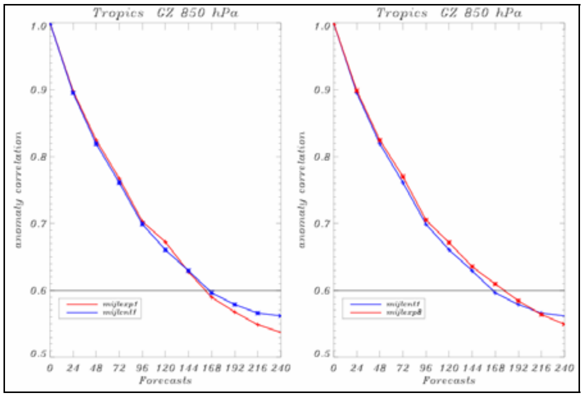

Figure 11. AC as a function of forecast length for tropical GZ at 850 hPa in July 2003. CNT1 (blue) vs. EXP1 (red) on left and CNT1 (blue) vs. EXP8 (red) on right.

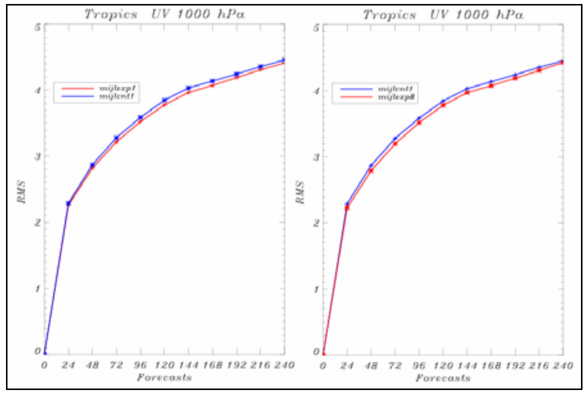

Figure 14. RMS error as a function of forecast length for tropical winds at 1000 hPa in July 2003. CNT1 (blue) vs. EXP1 (red) on left and CNT1 (blue) vs. EXP8 (red) on right.

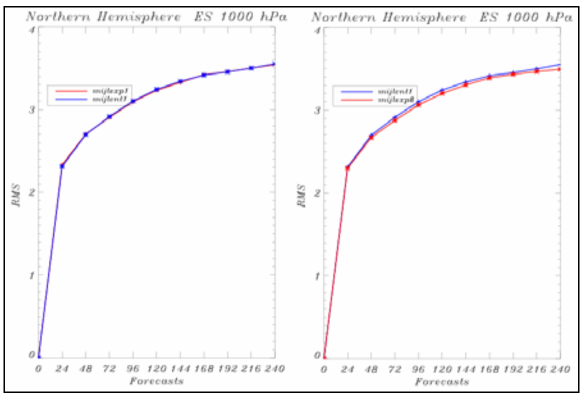

Figure 12. RMS error as a function of forecast length for NH ES at 1000 hPa in July 2003. CNT1 (blue) vs. EXP1 (red) on left and CNT1 (blue) vs. EXP8 (red) on right.

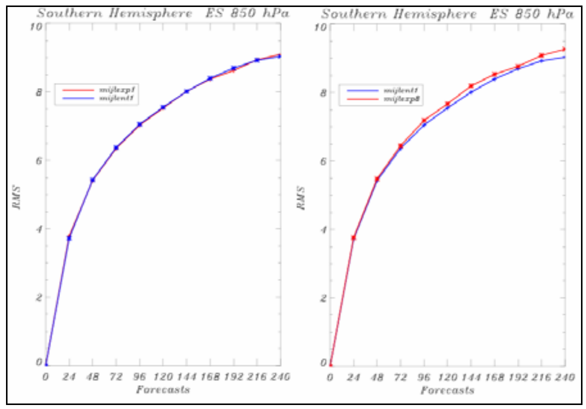

Figure 15. RMS error as a function of forecast length for SH ES at 850 hPa in July 2003. CNT1 (blue) vs. EXP1 (red) on left and CNT1 (blue) vs. EXP8 (red) on right.

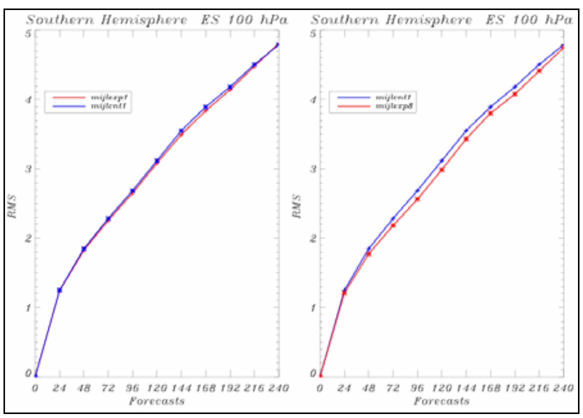

Figure 13. RMS error as a function of forecast length for SH ES at 100 hPa in July 2003. CNT1 (blue) vs. EXP1 (red) on left and CNT1 (blue) vs. EXP8 (red) on right.

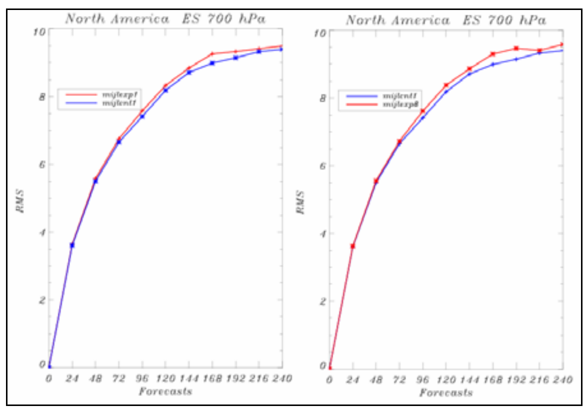

Figure 16. RMS error as a function of forecast length for NA ES at 700 hPa in July 2003. CNT1 (blue) vs. EXP1 (red) on left and CNT1 (blue) vs. EXP8 (red) on right.

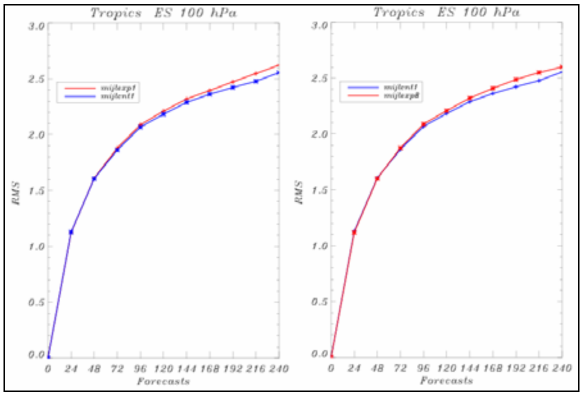

Figure 17. RMS error as a function of forecast length for tropical ES at 100 hPa in July 2003. CNT1 (blue) vs. EXP1 (red) on left and CNT1 (blue) vs. EXP8 (red) on right.

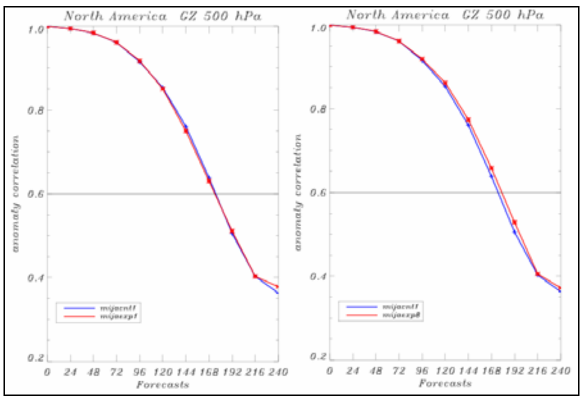

Figure 18. AC as a function of forecast length for NA GZ at 500 hPa in January 2004. CNT1 (blue) vs. EXP1 (red) on left and CNT1 (blue) vs. EXP8 (red) on right.

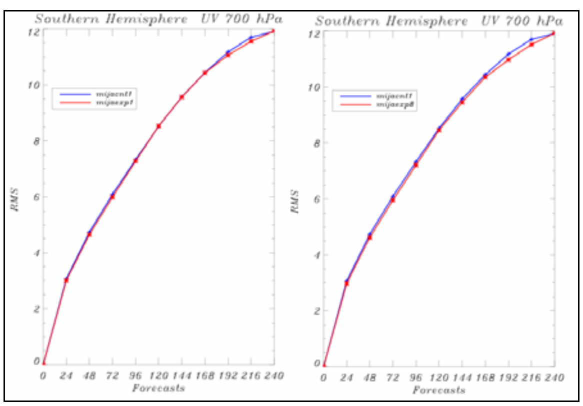

Figure 19. RMS as a function of forecast length for SH winds at 700 hPa in January 2004. CNT1 (blue) vs. EXP1 (red) on left and CNT1 (blue) vs. EXP8 (red) on right.

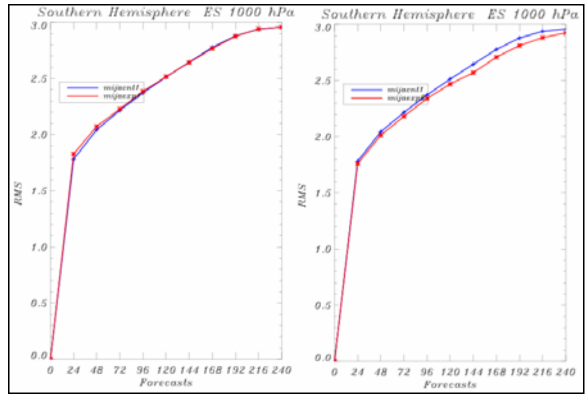

Figure 20. RMS as a function of forecast length for SH ES at 1000 hPa in January 2004. CNT1 (blue) vs. EXP1 (red) on left and CNT1 (blue) vs. EXP8 (red) on right.

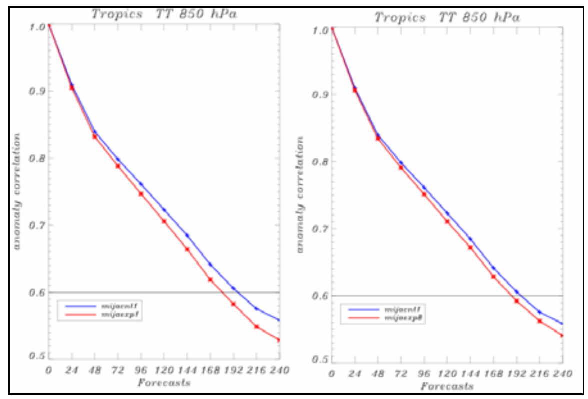

Figure 21. AC as a function of forecast length for tropical TT at 850 hPa in January 2004. CNT1 (blue) vs. EXP1 (red) on left and CNT1 (blue) vs. EXP8 (red) on right.

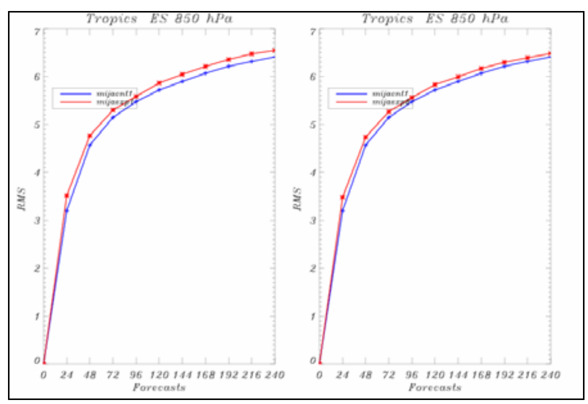

Figure 22. RMS as a function of forecast length for tropical ES at 850 hPa in January 2004. CNT1 (blue) vs. EXP1 (red) on left and CNT1 (blue) vs. EXP8 (red) on right.

first of these cases, the effect is attributed to EXP8 modifications, and in the last two it is attributed to the addition of SSM/I data.

For January 2004, there are impressive increases in the GZ AC at levels between 1000 and 300 hPa over the SH and NA (e.g. Fig. 18). Also over NA, improvements in TT AC are evident between 850 and 500 hPa. In the SH, there are reductions in the RMS error of the lower tropospheric winds (Fig. 19) and of the near-surface moisture field (Fig. 20). All of these improvements are associated with EXP8 only. The negative impacts include a decrease in TT AC (Fig. 21) and an increase in RMS error of ES (Fig. 22) in the lower troposphere of the tropics. It is significant that in these cases, EXP8 diminishes the degree of deterioration brought about by EXP1.

These results illustrate that for the forecasts, a greater positive impact is realized by the combination of adding SSM/I data and removing select AMSU observations, rather than by adding SSM/I data by itself. They also suggest that the gains made in the analyses by the addition of SSM/I data do not translate into significant gains in the forecasts until the filtering of AMSU data has been strengthened.

4.5 Verification of forecasts against analyses time series

Similar to the time series plots for forecasts versus RAOBS, there are not many strong positive or negative impacts evident in the charts using analyses as the validation set. A couple of exceptions are found in January for EXP8. For example, over the SH at 144h the GZ and ES fields show notable positive impacts at 500 hPa (Fig. 23) and 1000 hPa (Fig. 24), respectively.

4.6 Verification of forecast RMSE (2D maps)

A few of the changes to the forecasts discussed in the previous sub-sections are further illustrated by plotting geographically the difference between the RMS errors computed for the experiment versus its analysis and the control versus its analysis. These plots were created with respect to EXP8 since this experiment generates the most impact.

The deterioration in the July 850 hPa moisture field in the SH is evident in the 96h plot of ES (Fig. 25). For January, the dramatic improvements in 500 hPa GZ in the NH and SH are evident in the 96h plot (Fig. 26). Reductions in RMS error in the SH near-surface winds are also observed in the 96h map shown in Figure 27.

4.7 Verification of precipitation

A verification of the 24 hour accumulation of precipitation using the North American SYNOP and SHEF observation sets is performed for the two experiments in both seasons using bias and equitable threat scores. For July 2003, the SYNOP results show improvements in the 00h to 24h and 12h to 36h scores for EXP1 and EXP8 in the larger categories (e.g. Fig. 28). Otherwise, the experiments do not show much change from the control cycle. For January 2004, comparisons against the SHEF network indicate improvements in the 00 to 24, 12 to 36, 24 to 48, and 48 to 72 forecasts (e.g. Fig. 29), with a reduction in positive impact at longer forecast times.

4.8 Populations of assimilated observations

By comparing the number of observations assimilated for EXP1 and EXP8, the effectiveness of the AMSU-B channel 2 pseudo cloud filter applied in EXP8 is demonstrated. The global distribution of observations rejected by this filter over the month of July for AMSU-B channel 3 is plotted in Figure 30a. The distributions for channel 4 and 5 are similar. Globally, the filter results in a 7% reduction in the number of observations assimilated for each channel. Note that the areas outlined in pink match quite closely those areas in the CLW chart (Fig. 30b) that are characterized by persistent cloudiness. The surface rain rate chart (Fig 30c) indicates that these areas are not precipitating much of the time, such that the precipitation screen would rarely be active. Therefore, in the absence of the pseudo cloud filter, it is clear that many AMSU-B observations are currently assimilated in cloudy, non-precipitating conditions in the CMC's operational analysis system.

Other interesting effects on the number of AMSU-B observations assimilated occur as a result of adding SSM/I data. For both January and July, the number of AMSU-B CH2 observations assimilated between CNT1 and EXP1 increases by between 4-8%, mainly in the tropics (e.g. Fig. 31). The exceptions are small decreases in the marine stratocumulus (SC) regions located off the west coast of NA and South America. The general increase is due to a lower number of observations being removed during the background check, which filters data with large observation minus background values, when SSM/I data is assimilated. Thus, SSM/I data brings the trial fields closer to the AMSU-B CH2 observations. In the marine SC regions, the SSM/I data is guiding the trial fields away from AMSU-B CH2, which results in more filtering and less assimilation. This supports the conclusion that without the pseudo cloud filter, AMSU-B CH2 observations are assimilated in areas that they should not be. For other AMSU-B channels there is essentially no effect of adding SSM/I brightness temperatures.

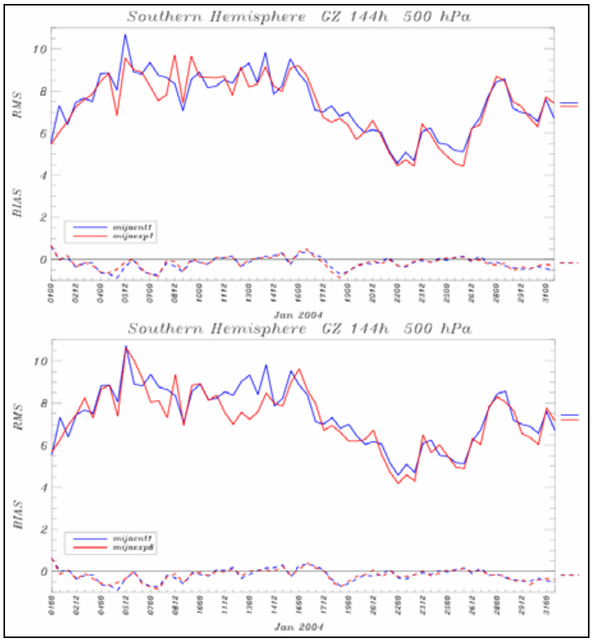

Figure 23. Time series of RMS error (solid lines) and bias (dashed lines) of 144h forecast vs. analyses for SH GZ at 500 hPa for January 2004. CNT1 (blue) vs. EXP1 (red) above and CNT1 (blue) vs. EXP8 (red) below.

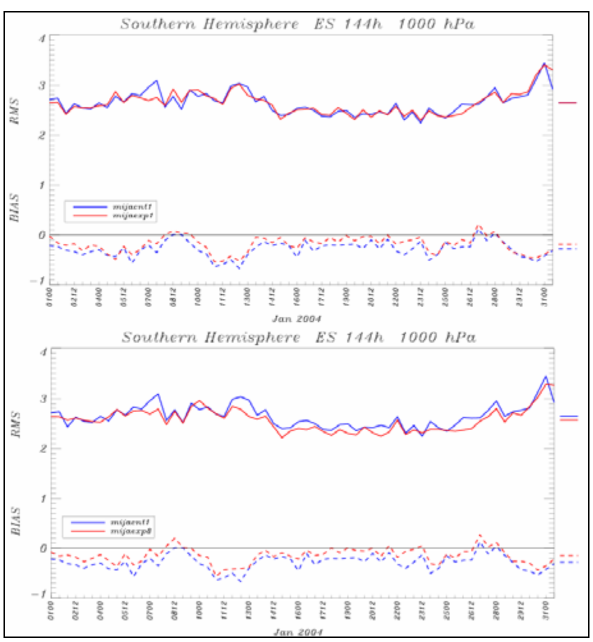

Figure 24. Same is in Figure 23, except for SH ES at 1000 hPa.

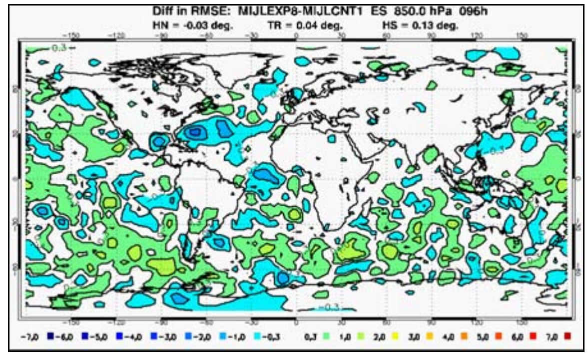

Figure 25. Difference in RMS error of 96h forecast vs. analysis between EXP8 and CNT1 for 850 hPa ES in July 2003. Blue (green) colors indicate areas where RMS error has been reduced (increased) in the experiment.

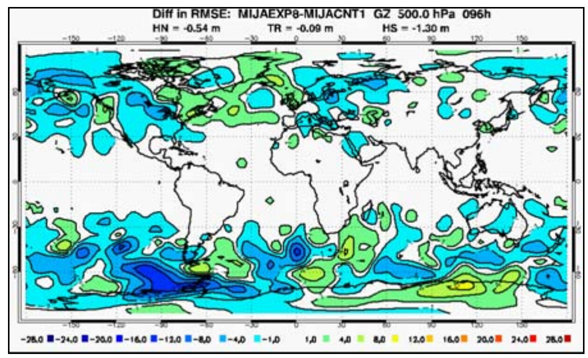

Figure 26. Same as in Figure 25, except for 500 hPa GZ in January 2004.

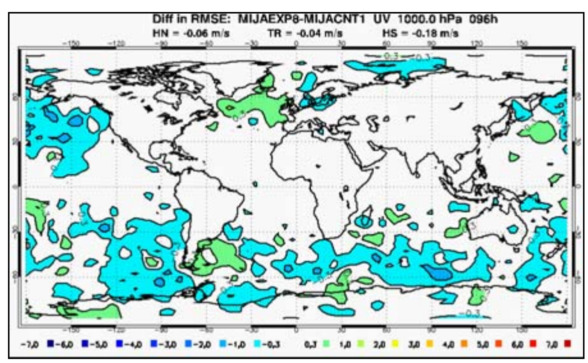

Figure 27. Same as in Figure 25, except for 1000 hPa winds in January 2004.

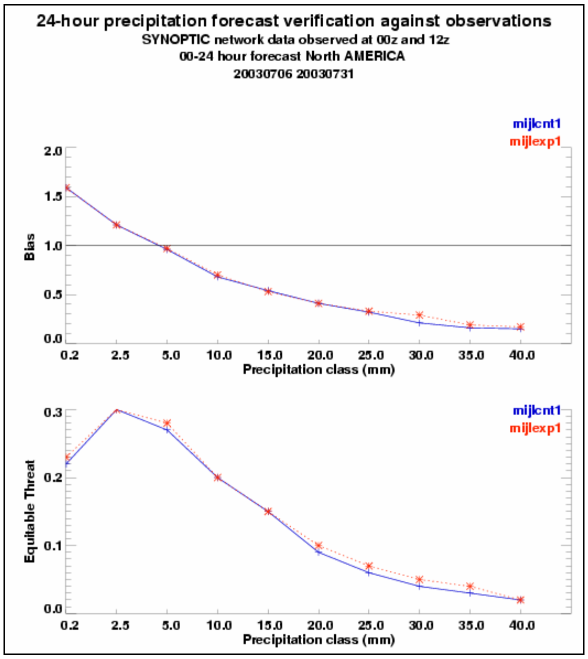

Figure 28. Bias and equitable threat scores for EXP1 24h QPF between 00h and 24h over NA computed using SYNOP observations at 00Z and 12Z in January 2003.

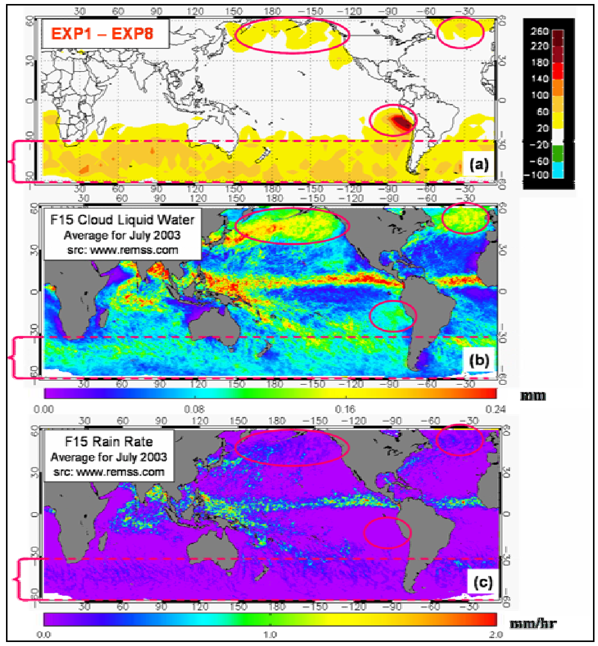

Figure 30. Difference in the number of observations assimilated for AMSU-B channel 3 between EXP1 and EXP8 (a). Mean CLW (mm) (b) and surface rain rate (mm hr^{-1}) (c) derived from DMSP-15 SSM/I observations for July 2003 (from Remote Sensing Systems: **www.remss.com**).

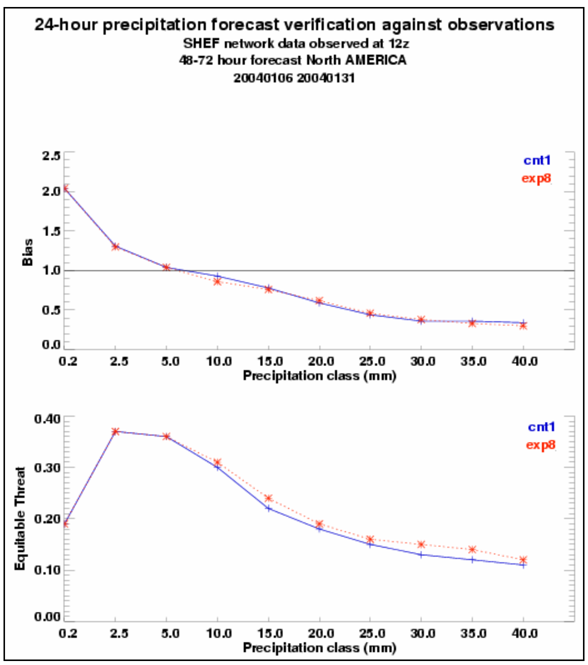

Figure 29. Bias and equitable threat scores for EXP8 24h QPF between 48h and 72h over NA computed using SHEF observations at 12Z in January 2004.

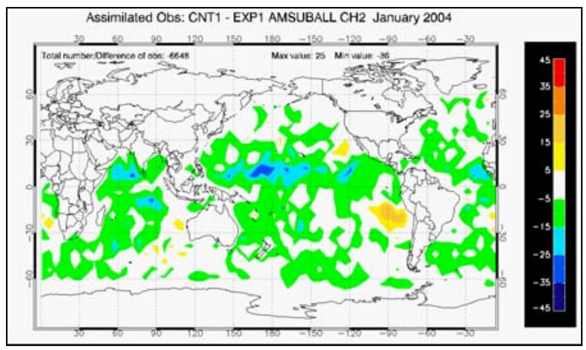

Figure 31. Difference in the number of observations assimilated for AMSU-B CH 2 between CNT1 and EXP1 for January 2004. Cold (warm) colors indicate where the number of observations has increased (decreased).

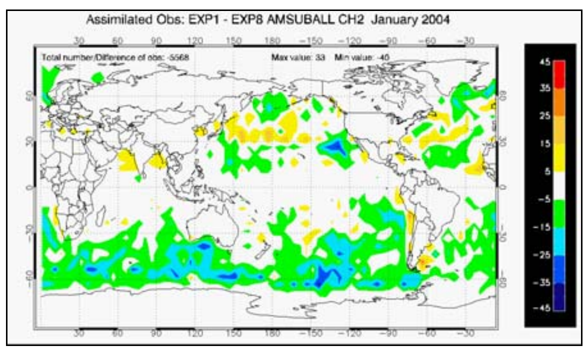

Figure 32. Same is in Figure 31, except the difference is computed between EXP1 and EXP8.

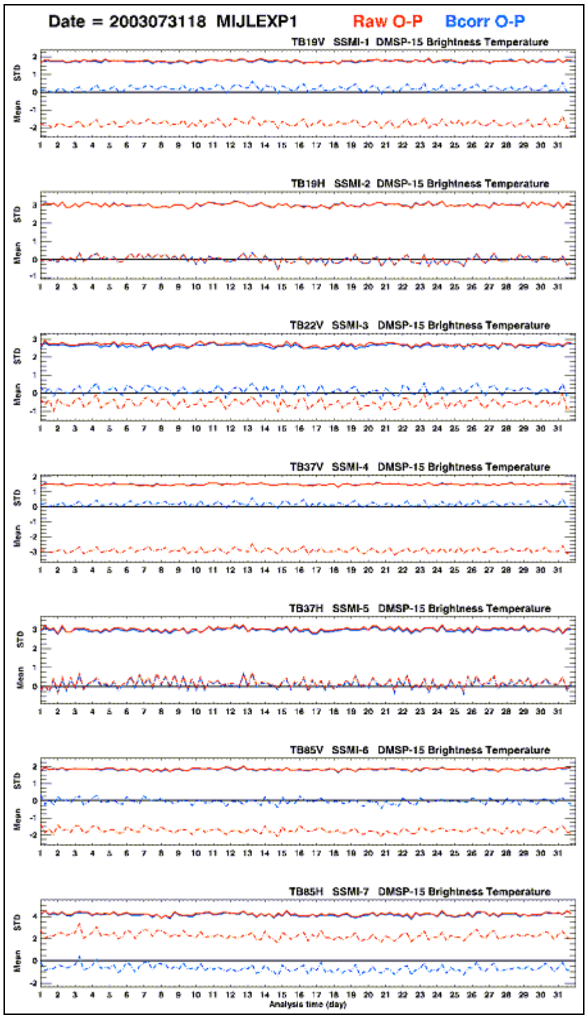

Figure 33. Bias (dashed lines) and standard deviation (solid lines) of observations minus first-guess before (red) and after (blue) the application of bias corrections. Statistics are shown for the seven SSM/I channels of DMSP-15 for EXP1 over the month of July 2003.

Additionally, after adding SSM/I data it is noted that with the extra filtering of AMSU-B data by the pseudo cloud filter, the number of observations assimilated for AMSU-B CH2 actually *increases* (comparing EXP1 and EXP8; Fig. 32). A global augmentation of about 1% and 2% is observed in July and January, respectively. Again, this suggests that by excluding the observations with innovations greater than 5 K, the trial fields are brought more in-line with the remaining CH2 observations which results in less filtering overall. In January, the increase is more dramatic in the SH mid-latitudes and the eastern Pacific Ocean, following the marine SC cloud pattern.

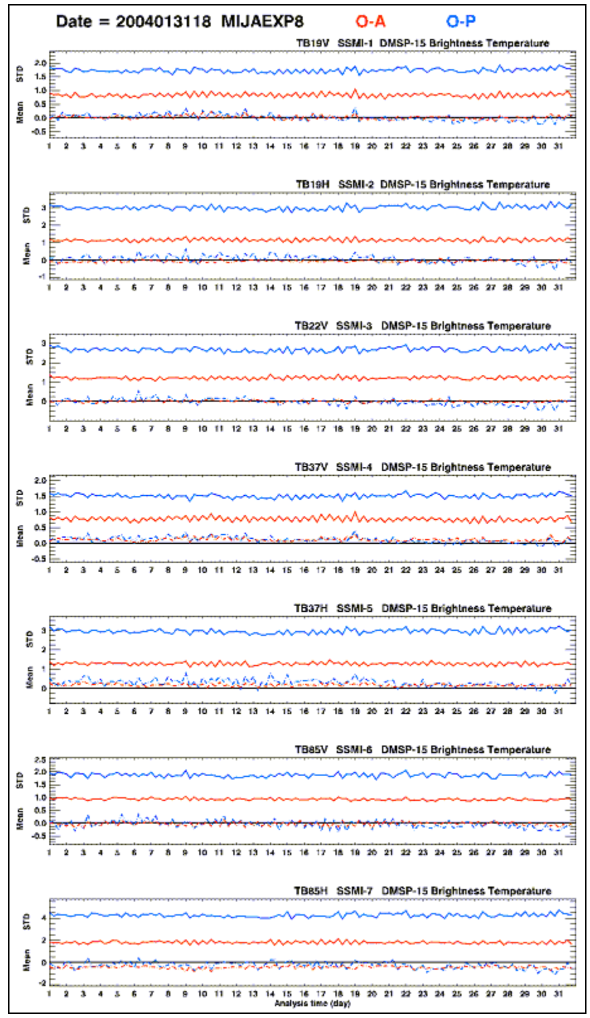

Figure 34. Bias (dashed lines) and standard deviation (solid lines) of observation minus first-guess (blue) and observation minus analysis (red) for the seven SSM/I channels of DMSP-15 for EXP8 over the month of January 2004.

4.9 Monitoring

For each of the experiments, typical monitoring procedures are applied. Figure 33 demonstrates that the bias corrections applied to the seven SSM/I channels of DMSP-15 in EXP1 for July 2003 are effective. In Figure 34, the expected reduction in the magnitude of SD from observation minus first-guess to observation minus analysis is illustrated for EXP8 during January 2004. Similar results are obtained for all DMSP satellites.

5 Conclusions

Brightness temperatures from three SSM/I polar orbiting instruments are assimilated in the CMC's 3D-Var scheme over two one month periods during July of 2003 and January of 2004. As a second experiment, more strict filtering of AMSU data is tested concurrently with the assimilation of SSM/I data. An important component of the enhanced filtering is the application of a pseudo cloud filter to AMSU-B observations. Currently, AMSU-B data is assimilated operationally at CMC after rejecting observations in areas of precipitation. However, observations in cloudy, non-precipitating areas are not removed by the quality control measures. It is shown in the second experiment that the application of a pseudo cloud filter results in the rejection of these observations. Therefore, it is highly recommended that this modification be implemented into operations.

The SSM/I instrument is an imager and so provides information on moisture below 500 hPa. Therefore, the SSM/I complements AMSU-B which provides information on atmospheric humidity from the surface to the upper troposphere. It has also been noted at ECMWF (G. Kelly, personal communication) that assimilating SSM/I data improves surface analyses, but not necessarily forecasts. Indeed, our experiments show that the addition of SSM/I data alone improves to the analysed IWV and SWS fields averaged over the month, however, the forecasts are not largely affected.

The addition of SSM/I data plus the removal of AMSU-A channel 3, and the rejection of cloudy observations for AMSU-B channels 2, 3, 4, and 5 provide the same positive impact found in EXP1, but with additional improvements to the forecasts. A few negative impacts are noted, however, these are less in number and magnitude than the improvements. It is possible that some of the gains that are observed in the EXP8 forecasts are actually due to the addition of SSM/I data, which has a stronger impact on the forecasts only after the suspicious AMSU data has been removed. Indeed, the impact on the forecasts due to the enhanced filtering of AMSU data is large considering the number of observations removed.

Maps of the number of observations assimilated in both experiments show that the addition of SSM/I data and the enhanced filtering of AMSU data both result in an increase in the number of net AMSU-B CH2 observations that are assimilated. This is a another indication that the assimilation system is improved by these changes.

Finally, the addition of SSM/I data is beneficial to the operational analysis system for two important reasons. First, the observations from the two independent observing systems, SSM/I and AMSU, are complementary which permits a more thorough sampling of the atmosphere. Second, an increase in the global coverage and number of quality satellite observations ingested should decrease the chances of missing extreme weather events.

6 References

Alishouse, J. C., S.A. Snyder, J. Vongsathorn, and R. R. Ferraro, 1990: Determination of oceanic total precipitable water from the SSM/I. *IEEE Trans. Geosci. Remote Sens*., **28**, 811-816.

Bennartz R., A. Thoss, A. Dybbroe, and D. B. Michelson, 2002: Precipitation analysis using the Advanced Microwave Sounding Unit in support of nowcasting applications. *Meteorol. Appl.*, **9**, 177-189.

Côté, J, S. Gravel, A. Méthot, A. Patoine, M. Roch, and A. Staniforth, 1997: The operational CMC-MRB Global Environmental Multiscale (GEM) model. Part 1: Design considerations and formulation. *Mon. Wea. Rev.*, **126**, 1373-1395.

Harris, B. A. and G. Kelly, 2001: A satellite radiance bias correction scheme for data assimilation. *J. R. Meteorol. Soc.*, **127**, 1453-1468.

Grody, N., J. Zhao, R. Ferraro, F. Weng, and R. Boers, 2001: Determination of precipitable water and cloud liquid water over oceans from the NOAA-15 advanced microwave sounding unit. *J. Geophys. Res.*, **106**, 2943-2953.

Petty, G. W., 1990: On the response of the SSM/I for atmospheric parameter retrievals. Ph. D. thesis, University of Washington, 252 pp.

Weng, F. and N. C. Grody, 1994: Retrieval of cloud liquid water using the Special Sensor Microwave Imager. *J. Geophys. Res.*, **99,** 14493–14502.